ORIGINAL ARTICLES

An integrated system for the complete segmentation of the common carotid artery bifurcation in ultrasound images

Christos P. Loizou[1], Marios Pantziaris[2]

1. Department of Computer Science, Intercollege, Limassol, Cyprus. 2. Cyprus Institute of Neurology and Genetics, Nicosia, Cyprus.

Correspondence: Christos P. Loizou. Address: Intercollege, 92 Ayias Phylaxeos Str., P.O. Box 51604, CY 3507 Limassol, Cyprus. Email: loizou.c@lim.intercollege.ac.cy; panloicy@logosnet.cy.net

Received: June 16, 2015 **Accepted:** July 14, 2015 **Online Published:** July 28, 2015
DOI: 10.5430/jbei.v1n1p11 **URL:** http://dx.doi.org/10.5430/jbei.v1n1p11

Abstract

The complete segmentation of the common carotid artery (CCA) bifurcation in ultrasound images is important for the evaluation of atherosclerosis disease and the quantification of the risk of stroke. The current research work further evaluates and validates a semi-automated (SA) snake's based segmentation system suitable for the complete segmentation of the CCA bifurcation in two-dimensional (2D) ultrasound images. The proposed system semi-automatically estimates the intima-media thickness (IMT), the atherosclerotic carotid plaque borders and dimensions, the internal carotid artery (ICA) origin's stenosis, the carotid diameter (D), as well as other geometric measurements of the atherosclerotic carotid plaque. The system was evaluated on 300 2D longitudinal ultrasound images of the CCA bifurcation with manual (M) segmentations available from a neurovascular expert. No statistical significant differences between all M and SA IMT, plaque and D segmentation measurements were found. In a future study, texture features extracted from the intima-media complex (IMC) may be used to separate subjects in high and low risk groups, which may develop a stroke. However, a larger scale study is required for evaluating the system before its application in the real clinical practice.

Key words

Intima-media thickness, Lumen carotid diameter, Carotid plaque, Carotid artery segmentation, Ultrasound imaging

1 Introduction

Atherosclerosis of the carotid artery is a pathological process mainly affecting the common carotid artery (CCA) bifurcation and is one of the major clinical manifestations leading to cardiovascular disease (CVD) [1]. It causes thickening of the artery walls and may develop atherosclerotic carotid plaques that causes stenosis in the artery lumen, thus affecting the normal blood flow [1-4]. Atherosclerosis can result in heart attack and stroke [1-3, 5].

Carotid intima-media-thickness (IMT) is a measurement of the thickness of the innermost two layers of the arterial walls. The IMT provides the distance between the lumen-intima and the media-adventitia [2, 5] (see Figure 1, bands Z5 and Z6 at the far wall of the CCA). A B-mode ultrasound image, shown in Figure 1, presents the intima-media complex (IMC) at the far wall of the CCA (echo zones Z5-Z6), as a pair of parallel bands, being one echodense and the other echolucent. The

leading edges I5 and I7 define the far-wall IMT. With this understanding, the determination of the IMT at the far wall of the artery becomes equivalent to accurately detecting the leading echo boundaries I5 and I7. It can thus be observed and measured as the double line pattern on both walls (far and near wall) of longitudinal ultrasound images of the CCA [6, 7] (see Figure 1). The IMT is used to measure and diagnose the extend of cardiovascular disease [1, 3-5]. Furthermore, the arterial lumen stenosis is a significant marker of atherosclerosis [4, 5]. It can be evaluated through the segmentation of the atherosclerotic carotid plaque [8-10] and the carotid lumen diameter (D) (see Figure 1, leading echo boundaries I4 and I5, band Z4). The measurements and follow up of the IMT, the atherosclerotic carotid plaque, the D, as well as grading of the internal carotid artery (ICA) stenosis, are imperative and are routinely assessed with high resolution ultrasound imaging of the CCA [11]. Traditionally, the above measurements are performed manually by experts and suffer from intra- and inter-observer variability [5-11]. Automated or semi-automated (SA) segmentation systems are therefore required which may reduce the time needed for the segmentation and increase the accuracy of the segmentation [6-12].

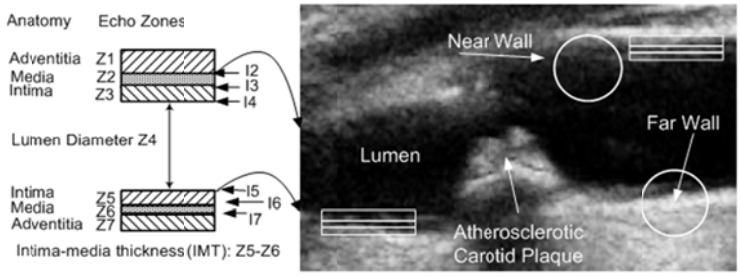

Figure 1. Illustration of the intima-media-complex (IMC) (bands Z5 and Z6), the atherosclerotic carotid plaque, at the far wall of the common carotid artery (CCA), the artery lumen diameter, D (band Z4), and the far and near walls of the CCA. The echo zones are also illustrated on the far and near walls on the image, which was acquired from a 69 year old symptomatic male subject at risk of stroke with 82% lumen stenosis. Figure is reproduced from Ref. [15] © IEEE TUFFC 2009.

A number of segmentation methods were proposed in the literature either for the segmentation of the IMC [6-9], the D [10, 12], the atherosclerotic carotid plaque [13, 14], or the media- and intima-layers [15], from ultrasound images of the CCA bifurcation. There are however, no other studies reported in the literature, where a complete segmentation of the CCA artery bifurcation has been presented. More specifically, a review [6] of different automated or SA techniques for the segmentation of the IMT, was reported while in a more recent study [16] a review on image and video segmentation studies of the CCA was presented. In Ref. [7], an IMC snake's based segmentation system was proposed, whereas in Ref. [15], the system proposed in Ref. [7], was further extended for segmenting the intima- and the media-layers in ultrasound images of the CCA by utilizing image normalization [17-20] and speckle reduction filtering [17]. Different CCA diameter indices were proposed in Ref. [10, 12], where the D was manually segmented and measured. In Ref. [13], a snakes based segmentation system was proposed for segmenting the atherosclerotic carotid plaque from CCA ultrasound images. In Ref. [15, 21], a small error between manual (M) and SA IMT snakes segmentation measurements was reported. Nakagami distributions were used in Ref. [22], while in Ref. [23], a multi resolution edge snapper was used to segment the IMC. The IMC was segmented in Ref. [24], using neural networks [25] with active contours and level sets. Hough transform and dual snake were used [26], while in Ref. [27] active contours were utilized for the IMC segmentation. Rocha et al. [14] proposed dynamic programming, while in Ref. [28, 29], two different 3D plaque segmentation methods based on level sets were presented. Finally, in Ref. [30] the IMT was assessed using the QLAB software while a lumen segmentation method was presented in Ref. [31].

All above systems were either proposed for the segmentation of the IMC, the D, or the atherosclerotic carotid plaque from ultrasound images of the CCA. Recently, a system for the complete segmentation of the CCA was proposed in Ref. [18] and evaluated on 20 two-dimensional (2D) ultrasound images, where preliminary results were reported. It is therefore still desirable the development of a segmentation system as proposed in this study, in which all the above aforementioned

techniques might be integrated together and applied in the clinical praxis. The clinical expert will thus be able to evaluate in a more precise and objective manner the risk of stroke in asymptomatic and symptomatic subjects at risk of atherosclerosis.

Our objective in this study was to further evaluate and validate on a larger sample of images, an SA complete integrated segmentation system [18] (see Figure 2) based on 2D snakes, for segmenting the IMC, the atherosclerotic carotid plaque and the D in 2D longitudinal ultrasound images of the CCA bifurcation. This will allow the introduction of the proposed system in the clinical practice. The proposed snakes segmentation system also utilizes image normalization and speckle reduction filtering in ultrasound images of the CCA trying to overcome some of the difficulties which arise during the segmentation process [6-15]. We have evaluated the proposed segmentation system on 300 ultrasound images of the CCA by comparing the SA segmentations with the M delineations made by a neurovascular expert.

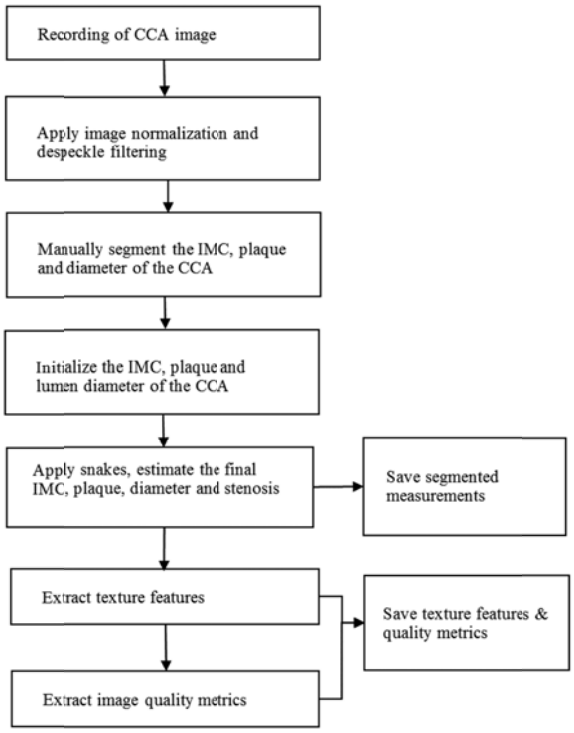

Figure 2. Flowchart analysis of the integrated system for the complete segmentation of the CCA in ultrasound imaging

2 Materials & methods

The following sections, which are also outlined in Figure 2, are only briefly described as all details can be found in Ref. [7, 13, 15-18, 32-34].

2.1 Recording of ultrasound images

In this study, three different sets of B-mode 2D longitudinal ultrasound images of the CCA bifurcation (300 images) were used, which were all acquired under the same protocol. The first image set (DB1) was used for the IMC and D segmentation and included 100 ultrasound B-mode images from symptomatic individuals, (40 women and 60 men) at a mean±SD (mean±standard deviation) age of 60.17±11.13 years and an ICA of 11.4±12.55%. Two of them had diabetes. The second image set (DB2), used for the atherosclerotic carotid plaque segmentation, included 100 ultrasound B-mode images (51 women and 49 men). They were acquired from symptomatic subjects at risk of atherosclerosis, with atherosclerotic carotid plaques of the CCA. The symptomatic subjects have already developed clinical symptoms, such as

a stroke or a transient ischemic attack and had a mean±SD age of 66.32±8.79 years and an ICA of 51.05±11.51%. The third image set (DB3), used for the IMC and D segmentation, included 100 ultrasound B-mode images (44 women and 56 men) acquired from normal subjects with no atherosclerotic disease. They had a mean±SD age of 38.11±7.56 years and an ICA of 9.2±12.3%. All images display the vascular wall as a regular pattern (see Figures 1-4), that correlates with anatomical layers. They were acquired by the ATL HDI-5000 ultrasound scanner (Advanced Technology Laboratories, Seattle, USA) [19] with a resolution of 576×768 pixels with 256 gray levels at the Cyprus Institute of Neurology and Genetics, in Nicosia, Cyprus. We use bicubic spline interpolation to resize all images to a standard pixel density of 16.66 pixels/mm (with a resulting pixel width of 0.06 mm) [20]. A written informed consent from each subject was obtained according to the instructions of the local ethics committee.

Before the segmentation of the IMC, plaque and D, of the CCA all images were manually normalized [20] (see Figures 3 and 4) and despeckled with the filter *DsFlsmv* introduced in Ref. [35] and evaluated in Ref. [7, 13-15, 18]. We present in Figure 4 the M (left column of Figure 4) and the SA segmentations (right column of Figure 4, see subsection II.D) of the CCA bifurcation after image normalization and despeckle filtering.

2.2 Manual IMC, plaque and diameter segmentation

The delineations were made by the neurovascular expert (co-Author M. Pantziaris) on all the 300 2D longitudinal ultrasound images of the CCA bifurcation, after image normalization and speckle reduction filtering. The IMT was measured by selecting 20 to 30 consecutive points for the intima and the adventitia layers at the far wall of the CCA. The D was measured by selecting 20 to 30 consecutive points at the two walls (see Figure 1, boundaries I4 and I5) of the CCA and points were perpendicularly connected between walls [36]. The atherosclerotic carotid plaque was measured by selecting 20-30 consecutive points forming a closed contour at the far or near wall of the CCA.

2.3 IMC, Plaque and lumen diameter contour initialization

Before running the IMC, plaque, and D snakes segmentation algorithm, different IMC [7, 15], atherosclerotic carotid plaque [13], and D [18], initialization procedures [7, 13, 15] were carried out for positioning the initial snake contours as close as possible to the area of interest. The segmentation initialization procedure is illustrated in Figure 3 and described in detailed in Ref. [18].

2.4 IMC, Plaque and diameter snakes segmentation

The IMC, the atherosclerotic carotid plaque and the D of the CCA, were segmented after normalization and despeckle filtering, using a snakes based segmentation system developed in MATLAB® [7, 13, 15]. The segmentations were based on the Williams & Shah [37] snake segmentation method, which was used to deform the snake and segment the IMC, the atherosclerotic carotid plaque and the near carotid wall borders in each image. The snake $v(s)$, adapts itself by a dynamic process that minimizes an energy function ($E_{snake}(v,s)$) defined as [37]:

$$E_{snake}(v(s)) = E_{\text{int}}(v(s)) + E_{image}(v(s)) + E_{external}(v(s)) = \int_s (\alpha_s E_{cont}(v(s)) + \beta_s E_{curv}(v(s)) + \gamma_s E_{image}(v(s)) + E_{external}(v(s)))\,ds \quad (1)$$

where $E_{\text{int}}(v(s))$, $E_{image}(v(s))$, $E_{external}(v(s))$, $E_{cont}(v(s))$, $E_{curv}(v(s))$ are the internal, image, external, continuity, and curvature energies of the snake, and $\alpha(s)$, $\beta(s)$ and, $\gamma(s)$ the strength, tension and stiffness parameters respectively. The method was introduced and evaluated in Ref. [7, 13, 15-18].

The extracted final SA contours (see Figure 4 right column), correspond to the adventitia and intima borders of the IMC at the far wall and the intima border at the near wall of the CCA as well as to the plaque borders. The D was then calculated

with the proposed integrated system also recently proposed in Ref. [18], in an area which was free of atherosclerotic plaques (see also Figure 4e and 4f). The distance is computed between the two boundaries (at the far wall for the IMT and at the near and far walls for the D), at all points along the arterial wall segment of interest moving perpendicularly between pixel pairs, and then averaged to obtain the mean IMT (IMTmean). Also the median (IMTmedian, Dmedian), IMT and D values, were calculated.

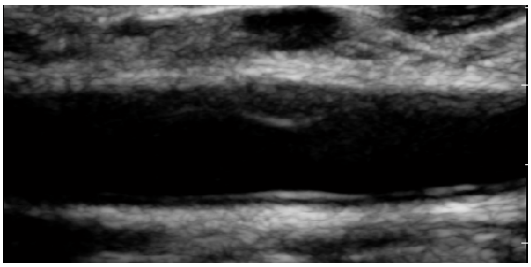

(a) Original ultrasound CCA image

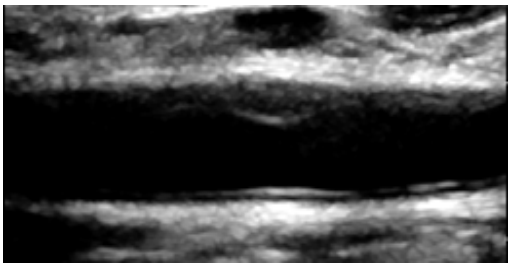

(b) Normalized despeckled CCA image

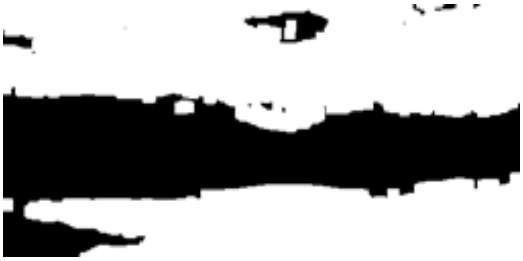

(c) Eroded binary CCA image

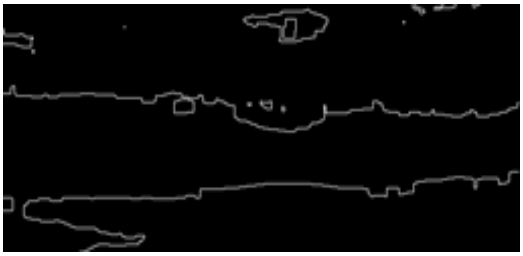

(d) Edge CCA image

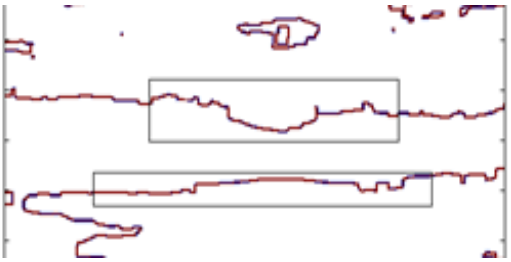

(e) ROI manual positioning, interpolating spline and contour selection

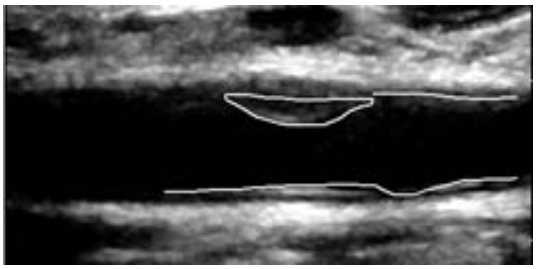

(f) Interpolating B-splines (initial snake contours)

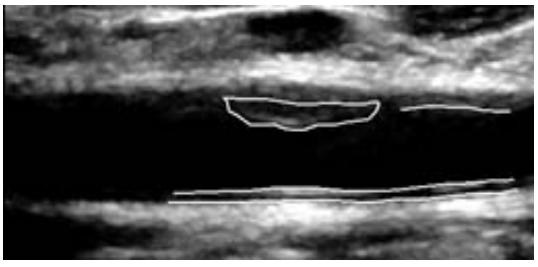

(g) Final SA CCA contours

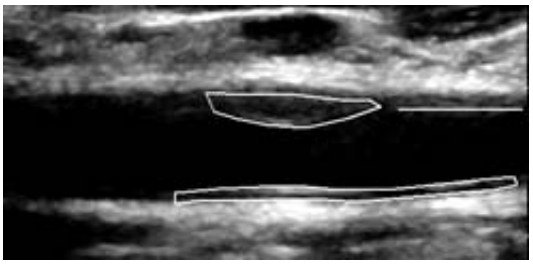

(h) M delineations of the CCA

Figure 3. Plaque contour initialization procedure and final snake contours: a) Original ultrasound CCA image, b) Normalized despeckled image with *DsFlsmv* filter (2 iterations, window 3×3), c) binary image after dilation with a square window shape of size 9×9 after removing edges, d) edge image after removal of erroneous edges, e) ROI's manual positioning, and interpolating splines and detected initial contours with contour selection, f) initial snake contours mapped on the image, g) final SA snake contours after snakes deformation, and h) M complete delineations of the CCA.

Finally, the ICA stenosis was estimated using the carotid stenosis index (CSI) [10, 36]:

$$CSI = (1 - \frac{N}{D}) * 100 \quad (2)$$

where N is the lumen diameter in maximum stenosis location, and D is the lumen diameter of distal CCA.

2.5 Statistical analysis

Details for the statistical analysis performed in this study can be found in Ref. [7, 13, 15-18]. For independent samples of same sizes the Wilcoxon rank-sum test [38] was used. The non-normality of the distributions was investigated with the Shapiro-Wilk test (p<.05) [39]. The Cohen's measure [40], was also used to estimate the practical significance of our results in cases where limited number of samples are used. We estimated a moderate value of around 0.42 for the most of our comparisons which indicates an acceptable practical significance. Also, the Spearman's correlation coefficient, ρ, between the M and the SA segmentation measurements, which reflects the extent of a linear relationship between two data sets with non-normal distributions, was investigated [39].

3 Results

Figure 4 illustrate two different examples of M (see Figure 4a and 4c) and SA (see Figure 4b and 4d) complete segmentations performed on ultrasound images of a CCA. We may observe that M, performed by the expert, and SA segmentations performed by the proposed snake's segmentation system, are very close.

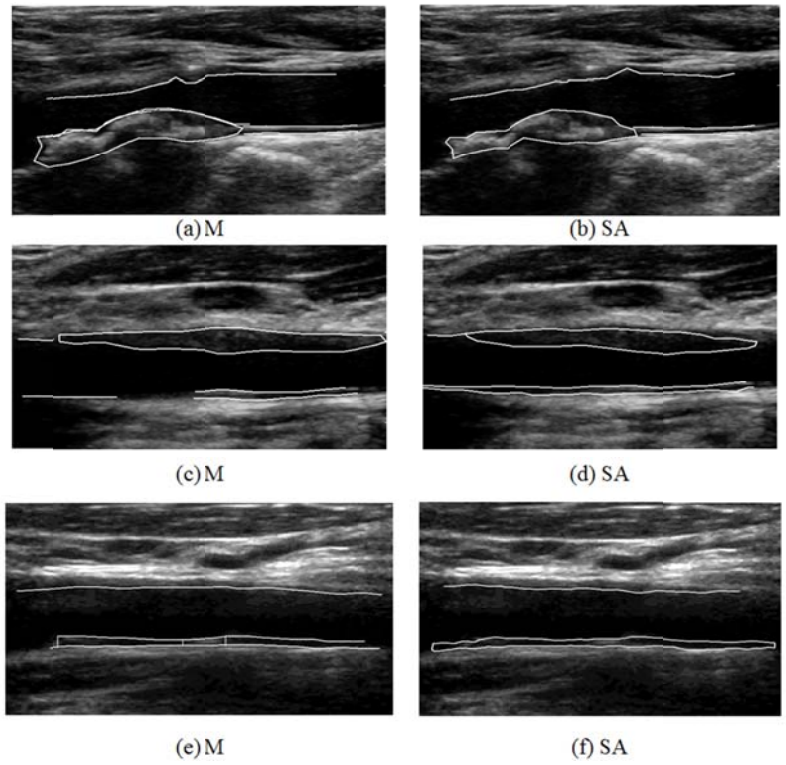

Figure 4. (a), (c),(e) M, and (b), (d) SA complete CCA segmentations in three different ultrasound images acquired from: Case 1 (in a), (b)): Male symptomatic subject at risk of stroke in the age of 53, Case 2 (in (c), (d)): Female symptomatic subject at risk of stroke in the age of 67. Case 3 (in (e) and (f)): Male normal individual at the age of 54. Segmentation measurements are shown in Table 1.

Table 1. M and SA IMT segmentation measurements (mm) for the CCA ultrasound images in Figure 4. Values are in (mm)

	Case 1		Case 2		Case 3	
	M	**SA**	**M**	**SA**	**M**	**SA**
IMT_{mean}	0.73	0.72	0.83	0.80	0.70	0.69
IMT_{median}	0.66	0.67	0.68	0.66	0.67	0.67
D_{mean}	5.51	5.65	5.45	5.51	5.81	5.90
D_{median}	5.78	5.75	5.56	5.49	5.73	5.77
ICA_{sten} (%)	47.4(12.4)	49.7(11.9)	38.8(14.4)	40.23(12.37)	-	-

Note. M: Manual, SA: Semi-automated, ICAsten: Internal carotid artery stenosis (mean [±SD])

Table 2 illustrates the M and the SA mean, SD and median segmentation measurements in millimeters for the IMT and D. These were performed on 200 subjects (100 normal + 100 diseased). We also present the percentage of ICA stenosis. Table 1 shows, that M and SA IMT and D segmentation measurements are close. Furthermore, we may observe that generally the M measurements exhibit larger variability when compared to the SA for both the IMT and D segmentation measurements. After performing the non-parametric Wilcoxon rank-sum test, we found no statistical significant differences between the M and the SA (mean, median) segmentation measurements, for both the IMT and the D (see last column of Table 2). We may observe that for both the IMT and the D measurements of the CCA, the values obtained from the normal group of subjects are generally smaller than those of the symptomatic patients for both the M and the SA segmentation measurements.

Table 2. Manual (M) and semi-automated (SA) mean, sd and median values for the IMC, d segmentation measurements and the ICA stenosis for the 100 normal subjects (normal) from DB3, and the 100 symptomatic (sympto) patients from DB1 investigated. Values are in (mm)

	CCA M segmentation measurements			CCA SA segmentation measurements			*p*-values (M *vs* SA) (mean/median)
	Mean	**SD**	**Median Q1/Q2/Q3**	**Mean**	**SD**	**Median Q1/Q2/Q3**	
IMT_{sympto}	0.96	0.32	0.80/0.97/1.02	0.95	0.22	0.84/0.93/1.04	.23/.42
IMT_{normal}	0.75	0.14	0.63/0.78/0.88	0.74	0.11	0.61/0.77/0.86	.77/.61
D_{sympto}	5.59	0.83	4.59/5.71/6.08	5.64	0.78	4.66/5.81/6.28	.72/.50
D_{normal}	4.74	0.86	4.22/4.72/5.18	4.83	0.82	4.28/4.79/5.21	.66/.49
ICA_{sten}	48.1%	11.52%	-	51.05%	11.51%	-	.33/-
ICA_{sten_normal}	-	-	-	9.2%	12.3%	-	-/-

Note. SD: Standard deviation, $IM_{Tnormal}$, D_{normal}, IMT_{sympto}, D_{sympto}: M and SA IMT and D segmentation measurements from all normal and symptomatic subjects investigated in this study, ICA_{sten_normal}, ICA_{sten}: Internal carotid artery stenosis for the normal and the symptomatic group of subjects. Q1, Q2, Q3: Quartile ranges Q25%, Q50%, Q75% respectively. The *p*-values refer to Wilcoxon rank sum test performed on the mean and median M *vs.* SA measurements at $p<.05$.

Figure 5 presents box plots for the mean and median M (_m), SA and the normal group segmentation measurements of the CCA for the IMT (see Figure 5a), and the CCA diameter, D (see Figure 5b), performed on the first (DB1) and third image (DB3) databases (100 symptomatic subjects and 100 normal subjects). M and SA segmentation measurements are very close.

Table 3 presents the Wilcoxon rank-sum test and the Spearman correlation coefficient, ρ, between the M and SA IMT (-/) and D (/-) segmentation measurements for all 100 symptomatic patients (DB1) and all 100 normal (DB3) subjects investigated in this study. We found no statistical significant differences between the M and the SA segmentation measurements, performed on the symptomatic subjects, as well as relatively higher ρ, between the M and SA segmentation measurements, for both the IMT and D measurements. We also found significant differences for all IMT and D measurements between the normal and the symptomatic SA as well as between the normal and the M segmentation measurements. Furthermore, we estimated generally lower correlation coefficients, ρ, for both the M and the SA segmentation measurements performed on the symptomatic subjects, when compared with the segmentation

measurements performed on the normal subjects. The present findings indicate a strong relationship between the M and the SA segmentation measurements and that the IMT and D SA segmentations may be as reliable as the M.

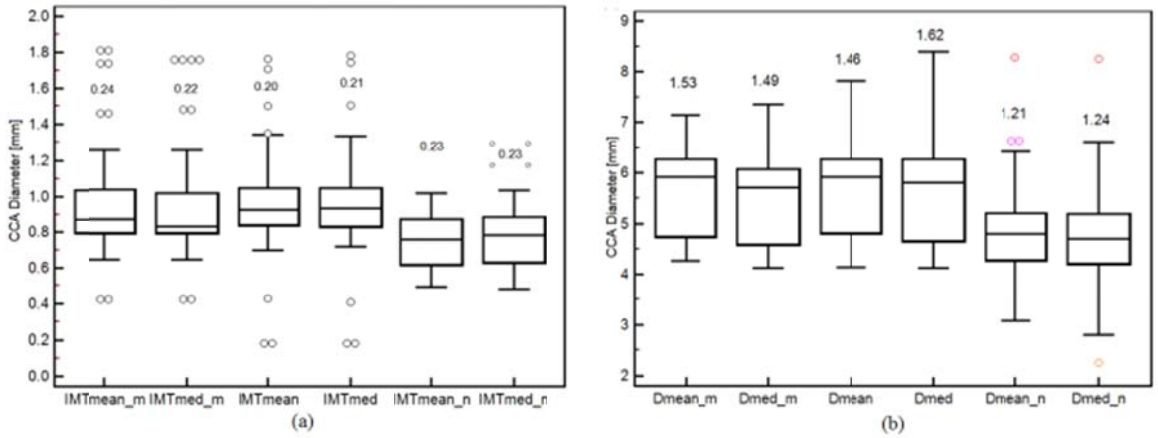

Figure 5. Box plots for the mean and median segmentation measurements of the CCA for the: (a) IMT, and (b) CCA D in millimeters (mm). From left to right, we present the mean (mean) and median (med) M (_m), SA and normal (_n) IMT and D segmentation measurements for the 100 symptomatic subjects of the first image dataset (DB1) and the 100 normal subjects (DB3) investigated. Inter-quartile range (IQR) values are shown above the box plots. Straight lines connect the nearest observations with 1.5 of IQR of the lower and upper quartiles. Unfilled circles indicate possible outliers with values beyond the ends of the 1.5×IQR.

Table 3. Wilcoxon rank-sum test performed, between the images from DB1 and DB3 (200 images), at $p<.05$ with star indicating significant different values and Spearman's correlation coefficient, ρ, with p in brackets for IMT (-/) and D (/-) segmentation measurements

		M, Normal		**SA, Symptomatic**		**M, Symptomatic**	
		Mean	**Median**	**Mean**	**Median**	**Mean**	**Median**
M, Symptomatic	Mean	*0.04(0.78) / *0.07(0.69)		0.16(0.67) / 0.21(0.72)			
	Median		*0.05(0.75) / *0.14(0.8)		0.19(0.74) / 0.33(0.86)		
SA, Symptomatic	Mean	*0.12(0.24) / *0.19(0.37)					
	Median		*0.19(0.67) / *0.09(0.34)				
SA, Normal	Mean	0.15(0.67) / 0.39(0.88)		0.24(0.55) / 0.37(0.52)		*0.14(0.31) / *0.39(0.42)	
	Media		0.33 (0.81) / 0.59(0.47)		0.16(0.81) / 0.47(0.16)		*0.25(0.83) / 0.17(0.21)

Note. M, SA: Manual, semi-automated measurements, *: Significantly different at $p<.05$, No *: Non-significantly different at $p\geq.05$

Table 4 tabulates the quantitative plaque segmentation results of the statistical analysis based on the specificity, sensitivity, the similarity kappa index (KI), and the overlap index for the proposed snakes segmentation method performed on all 100 ultrasound images of the CCA acquired from symptomatic subjects (DB2). We report mean±SD, and median values. The

results of the plaque SA segmentation method are compared with the M tracings of the expert which are considered to be the ground truth. The results show that the proposed method agrees with the expert by correctly detecting no plaque (Specificity) in (92.1.7±7.6)% of the cases and by correctly detecting a plaque (Sensitivity) in (85.42±8.1)% of the cases. The KI, and the overlap index, for the proposed snakes segmentation method were 84.6% and 74.7% respectively. It should be further noted that the snake contour may be attracted occasionally to local minima and converge to a wrong location. This occurred in less than 7% of the cases (*i.e.* in 7 images).

In Table 5, we illustrate the geometric measurements for the CCA bifurcation plaque for both the M and the SA segmentation measurements for all the 100 symptomatic images investigated (DB2). Last column of Table 5 illustrates the Wilcoxon rank-sum test performed between the mean and median values of the M and SA segmentation measurements.

Table 4. ROC analysis on Specificity, Sensitivity, Similarity kappa index (KI) and Overlap index for the atherosclerotic carotid plaque SA snakes segmentation method on 100 ultrasound images of the CCA bifurcation acquired from symptomatic subjects of the DB2 dataset. Values are reported in (mean±sd) (-/) and median (/-)

System detects	Expert detects no plaque (%)	Expert detects plaque (%)	KI (%)	Overlap Index (%)
No Plaque	Specificity=(92.1±7.6) / 90.3			
Plaque		Sensitivity=(85.42±8.1) / 84.9	84.6±6.1 / 83.7	74.7±4.1 / 75.2

Table 5. Manual (M) and snakes automated (SA) mean, sd and median geometric measurements for the CCA atherosclerotic plaque segmentation for the 100 symptomatic subjects of the DB2 investigated. Values are in (mm)

Geometric Measures	CCA M segmentation			CCA SA segmentation			*p*-values (M *vs.* SA) (mean/median)
	Mean	SD	Median	Mean	SD	Median	
Perimeter	50.3	20	55.4	48.9	20	56.2	0.48/0.65
Area	528.3	30	512	520.79	30	527	0.45/0.75
Dx-axis	22.5	9.8	25.4	21.66	9.6	25.2	0.39/0.89
Dy	4.3	1.6	4.2	4.19	1.6	4.0	0.61/0.84

Note. SD: Standard deviation, Dx, Dy: Diameter x-axis and y-axis. The *p*-values refer to Wilcoxon rank sum test performed on the mean and median M *vs.* SA segmentation measurements at $p<.05$

Finally, Figure 6 illustrates a Bland-Altman plot between the M and the SA mean segmentation IMT measurements (DB1). M and SA IMT segmentation measurements are very close demonstrating a difference of (0.01+0.82) mm and (0.01-0.80) mm. Similar findings were found for the D of the CCA.

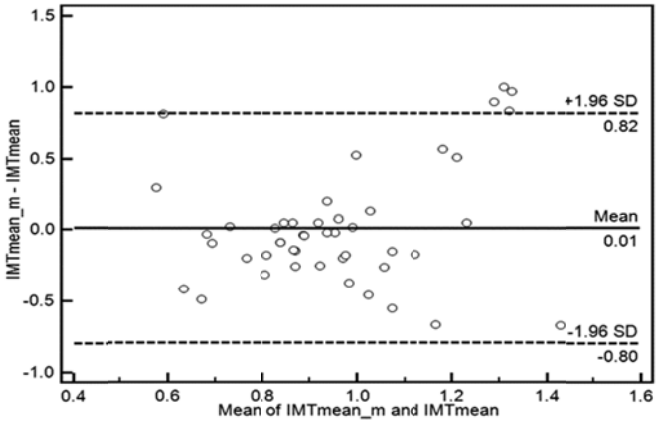

Figure 6. Regression lines (Bland–Altman plots) between the M (IMT_{mean_m}) and the SA mean IMT measurements (IMT_{mean}) for the 100 symptomatic subjects of the first image dataset (DB1) investigated. The middle line represents the mean difference, and the upper and lower two outside lines represent the limits of agreement between the two measurements, which are the mean of the data±2SD for the estimated difference between the two measurements.

4 Discussion

We integrated in this study three different segmentation techniques together into an integrated snake's based segmentation system and further validated the system in 300 ultrasound images from three different databases, of the CCA bifurcation. The system is able to segment the IMC, the D, and the atherosclerotic carotid plaque as well as to estimate the ICA stenosis. The three different structures (IMC, D and atherosclerotic plaque) are important for the clinical expert in order to correctly evaluate the degree of stenosis and the severity of the atherosclerosis disease in an asymptomatic or symptomatic individual at risk of stroke. It should be noted that the SA segmentation system proposed in this study is suitable for the complete segmentation of the CCA bifurcation in ultrasound images.

The results of this study showed that there are no statistical significant differences (see Tables 2 and 3) between the M and the SA segmentation measurements for the IMT, the D, and the atherosclerotic carotid plaque (see Table 4). The differences found in this study between the M and the SA segmentation measurements (see Table 2, Figures 5 and 6) are in general small, as also reported in other studies for the IMT [6-9, 41], the D [10, 12], and the atherosclerotic carotid plaque [13, 14]. Furthermore, it was shown in this study that the SA segmentation measurements for the IMT, the atherosclerotic plaque and D are very close to the M segmentation measurements (see Tables 2-5) as also reported in Ref. [6-15].

As shown in Table 2, the mean IMT for the symptomatic subjects (IMT_{sympto}) was for the M measurements (0.96±0.32) mm while for the SA measurements was (0.95±0.22) mm. In both cases (M and SA) higher values were estimated when compared with the values estimated for the normal group of subjects (IMT_{normal}: (0.75±0.14) mm *vs.* (0.74±0.11) mm for the M *vs.* SA respectively) [41]. This may be attributed to the fact that the patients investigated in this study were symptomatic at risk of atherosclerosis with relative high age (66.32±8.79 years old). Similar findings were also reported in Ref. [6-9, 41, 42]. It has also been reported in the literature [6-9, 15, 20, 37], that normal IMT values lies between 0.6 mm and 0.8 mm and that symptomatic subjects at risk of atherosclerosis exhibit higher IMT values [41, 43]. The D, as well as the ICA stenosis (9.2%) found in this study for the normal individuals are also consistent with results in Ref. [10-12] and are considered to lie within the normal range of values.

The ρ between the M and the SA measurements found in our study was not high (see Table 3), while ρ=0.86 [44], ρ=0.72 [45] with lower SD for the SA method, ρ=0.74 [46], whereas where 2,146 participants took place ρ=0.34 [47]. In Ref. [48, 49] a larger ρ=0.8 was reported where IMT was less than 0.9 mm. The difference in the agreement between those studies and our study may also be explained due to the different study settings, the study population, different observers, and a different way of ranking. It should be however noted that differences across studies in study populations may explain part of the findings. In most of the earlier studies, the study population consisted of healthy, young subjects. At younger ages, carotid IMT is more similar along a section of the carotid artery. Consequently, measurements in the CCA may tend to be more similar, and thus better agreement is found. The present study was performed in older patients with manifest vascular disease.

From Table 3, we may also observe that the agreement between the M and the SA plaque segmentations is good and that the system agrees with the expert in (85.42±8.1)% of the cases for non-detecting a plaque and in (92.1±7.6)% of the cases for detecting a plague. Additionally, a higher Williams index (84.6%) and a higher overlap (74.7%) was reported is this study in comparison with Ref. [13], performed on 80 ultrasound images of the CCA for the segmentation of the atherosclerotic carotid plaque, where lower values were reported (Williams index=80.66%, Overlap=69.3%). Rocha *et al.* also reported a sensitivity of 95% by segmenting the atherosclerotic carotid plaque using dynamic programming [14]. A number of other studies investigated segmentation of the CCA plaque [16], and their results are comparable with those found in this study. We can thus conclude that the SA measurements performed in this study are as much reliable and accurate as the M measurements performed by the neurovascular expert and therefore the system might be used in the clinical praxis. Specifically the system can aid the physician in carrying out the segmentation task. It is clearly stated that it is not the purpose of the system to replace the physician but to support it at its best.

The main conclusions resulting from this study were supported by other independent investigations which reveal that an IMT higher than 0.9 mm-1.0 mm [10-15] indicates potential atherosclerotic disease, which translates into an increased risk of a CVD event. Hence, the robust segmentation and measurement of the IMT as well as the atherosclerotic carotid plaque by B-mode ultrasound has a considerable impact in the early diagnosis of atherosclerosis, prognosis evaluation and prediction, and in the monitoring of response to lifestyle changes and to prescribed pharmacological treatments [1, 2].

We also found in this study, as well as in other studies performed by our group [7, 15, 32] an increase of carotid IMT with age and this is also in accordance with other studies [51, 52]. This increase of IMT with age reflects a progression of athero/ arteriosclerotic changes following a natural ageing process.

Compared with normal subjects, symptomatic patients at risk of atherosclerosis had increased CCA D (see Table 2: 5.59±0.83 *vs.* 4.74±0.86 mm; $p<.001$), and larger CCA IMT (0.96±0.32 mm *vs.* 0.75±0.14 mm; $p<.001$). A small D reflects to a healthy vasculature that is able to maintain an optimal balance of shear and tensile stress [53]. An enlarged D is less able to effectively control levels of shear stress. This can make the artery vulnerable to injury and atherosclerotic development [54]. It should be finally noted that the time required for the proposed segmentation system to fully segment the CCA bifurcation is about 35 seconds.

It should be finally noted that the system evaluated in this study has been also proposed in Ref. [18] where only a small set of image were used to evaluate the system. The relative large number of ultrasound images used (300 images) in this study further validates the system.

A number of limitations are discussed in Ref. [7, 13, 15-18] by also taking into consideration the follow up of the patients as well as take into account additional variables, such as age, sex, weight, blood pressure and others for better evaluating the risk of stroke in this group of patients. Acoustic shadowing, speckle noise [6, 7, 13, 17], as well as extensive echolucency, calcification and the positioning of the initial snake contour as it was discussed in Ref. [7, 13, 15-18], may cause additional problems in the processing of the images.

In a future work we will investigate a possible incorporation of the proposed SA segmentation system into a commercial computer aided diagnostic system that supports the texture image analysis of the segmented IMC and plaque areas, as documented in Ref. [32]. Furthermore, the motion characteristics of the arterial wall in ultrasound videos of the CCA [33], wall stress parameters of the atherosclerotic plaque [34] and environmental and genetic factors that may influence the development of plaques [55] may investigated. Furthermore, to incorporate the extraction of texture features [56, 57] from the IMC and the atherosclerotic carotid plaque, from ultrasound images and or videos which can be used to separate subjects in high and low risk groups for developing a stroke as it was also shown in Ref. [32, 57]. Finally, the use of despeckle filtering in ultrasound image [58] and video [59] segmentation of the atherosclerotic carotid plaque could be investigated for increasing the visual performance, and the M as well as the SA image and video segmentation accuracy of the IMC and plaque [33] of the CCA in this group of subjects.

5 Concluding remarks

In this work we integrate different existing 2D snakes based segmentation techniques together for the IMT, plaque and D segmentation and validated the system in 300 ultrasound images. We found no statistical significant differences between all M and SA segmentation measurements of the CCA. We thus anticipate that the proposed system might be used in the clinical praxis to complement M measurements. It should be noted that the SA integrated segmentation system proposed in this study is suitable for the complete segmentation of the CCA. We also anticipate in the future to apply the proposed system in a larger group of subjects and to extract texture characteristics from the segmented areas (IMC, media layer and carotid plague). These texture characteristics can then be used to classify or separate subjects with increased IMC structures, as it was shown in Ref. [32], as well separate normal and disease subjects, in different risk groups. Additionally,

features extracted from the atherosclerotic carotid plaque, may be used for the separation between asymptomatic and symptomatic subjects. However, a larger scale study is required for evaluating the system before its application in the real clinical praxis as an aid to the physician.

References

[1] Mendis S, Puska P, Norrving B. Global Atlas on cardiovascular disease prevention and control. WHO ISBN: 978-92-4-156437-3. 2012.

[2] Go S, Mozaffarian D, Veronique LR, *et al*. Heart disease and stroke statistics-2013 update: A report from the American Heart Association. Circulation. 2003; 127: e6-e245. PMid:23239837. http://dx.doi.org/10.1161/CIR.0b013e31828124ad

[3] Rothwell PM, Gibson RJ, Slattery J, *et al.* Prognostic value and reproducibility of measurements of carotid stenosis. A comparison of three methods on 1001 angiograms. European carotid surgery trialists' collaborative group. Stroke. 1994; 25: 2440-4. PMid:7974587. http://dx.doi.org/10.1161/01.STR.25.12.2440

[4] ACAS clinical advisory. Carotid endarterectomy for patients with asymptomatic internal carotid artery stenosis. Stroke. 1994; 25(12): 2523-4. PMid:7974602. http://dx.doi.org/10.1161/01.STR.25.12.2523

[5] Executive Committee for the Asymptomatic Carotid Atherosclerosis study, Endarterectomy for asymptomatic carotid stenosis. J. Am. Med. Assoc. 2002; 273: 1421-28.

[6] Molinari F, Zeng G, Suri JS. A state of the art review on intima-media thickness measurement and wall segmentation techniques for carotid ultrasound, Comp. Meth. Progr. Biomed. 2010; 100: 201-21. PMid:20478640. http://dx.doi.org/10.1016/j.cmpb.2010.04.007

[7] Loizou P, Pattichis CS, Pantziaris M, *et al.* Snakes based segmentation of the common carotid artery intima media. Med. Biol. Eng. Comput. 2007; 45: 35-49. PMid:17203319. http://dx.doi.org/10.1007/s11517-006-0140-3

[8] Molinari F, Meiburger KM, Saba L, *et al*. Constrained snake vs conventional snake for carotid ultrasound automated IMT measurements on multi-center data sets. Ultrasonics. 2012; 52: 949-61. PMid:22482369. http://dx.doi.org/10.1016/j.ultras.2012.03.005

[9] Xu X, Zhoua Y, Cheng X, *et al.* Ultrasound intima–media segmentation using Hough transform and dual snake model. Comput. Med. Imag. Graph. 2012; 36: 248-58. PMid:21741209. http://dx.doi.org/10.1016/j.compmedimag.2011.06.007

[10] Bladin F, Alexandrov AV, Murphy J, *et al.* Carotid stenosis index. A new method of measuring internal carotid artery stenosis. Stroke. 1995; 26: 230-4. PMid:7831693. http://dx.doi.org/10.1161/01.STR.26.2.230

[11] Nicolaides N, Sabetai M, Kakkos SK, *et al.* The asymptomatic carotid stenosis and risk of stroke study. Int. Angiol. 2003; 22(3): 263-72. PMid:14612853.

[12] Eigenbrodt ML, Sukhija R, Rose KM, *et al*. Common carotid artery wall thickness and external diameter as predictors of prevalent and incident cardiac events in a large population study. Cardiov. Ultras. 2007; 5(11): 1-11.

[13] Loizou P, Pattichis CS, Pantziaris M, *et al.* An integrated system for the segmentation of atherosclerotic carotid plaque. IEEE Trans. Inform. Techn. Biomed. 2007; 11(6): 661-7. PMid:18046941. http://dx.doi.org/10.1109/TITB.2006.890019

[14] Rocha R, Campilho A, Silva J, *et al.* Segmentation of the carotid intima-media region in B-mode ultrasound images. Image Vision Comput. 2010; 28: 614-25. http://dx.doi.org/10.1016/j.imavis.2009.09.017

[15] Loizou CP, Pattichis CS, Nicolaides AN, *et al.* Manual and automated media and intima thickness measurements of the common carotid artery. IEEE Trans. Ultras. Ferroel. Freq. Contr. 2009; 56(5): 983-94. PMid:19473916. http://dx.doi.org/10.1109/TUFFC.2009.1130

[16] Loizou CP. A review on ultrasound common carotid artery image and video segmentation techniques. Med. Biol. Eng. Comput. 2014; 52(12): 1073-93. PMid:25284219. http://dx.doi.org/10.1007/s11517-014-1203-5

[17] Loizou CP, Pattichis CS, Christodoulou CI, *et al.* Comparative evaluation of despeckle filtering in ultrasound imaging of the carotid artery. IEEE Trans. Ultras. Ferroel. Freq. Contr. 2005; 52(10): 1653-69. http://dx.doi.org/10.1109/TUFFC.2005.1561621

[18] Loizou CP, Kasparis T, Spyrou C, *et al.* Integrated system for the complete segmentation of the carotid artery bifurcation in ultrasound images. Presented at IFIP Int. Federation for Inform. Proc, 9th Int. Conf. Artific. Intellig. Applic. & Innov. (AIAI 2013) IFIP AICT 412, Pafos, Cyprus, Sept. 30 - Oct. 2, 292-301. http://dx.doi.org/10.1007/978-3-642-41142-7_30

[19] A Philips Medical System Company. Comparison of image clarity, SonoCT real-time compound imaging versus conventional 2D ultrasound imaging. 2001. ATL Ultrasound Report.

[20] Elatrozy T, Nicolaides AN, Tegos T, *et al.* The effect of B-mode ultrasonic image standardization of the echodensity of symptomatic and asymptomatic carotid bifurcation plaque. Int. Angiol. 1998; 17(3): 179-86. PMid:9821032.

[21] Faita V, Gemignani E, Bianchini C, *et al.* Real-time measurement system for evaluation of the carotid intima-media thickness with a robust edge operator. J. Ultrasound Med. 2008; 27(9): 1353-61. PMid:18716145.

[22] Meunier DJ, Giroux MF, Soulez G, *et al*. Segmentation in ultrasound B-mode images of healthy carotid arteries using mixtures of Nakagami distributions and stochastic optimization. IEEE Trans. Med Imag. 2009; 28(2): 215-29. PMid:19068423. http://dx.doi.org/10.1109/TMI.2008.929098

[23] Molinari C, Pattichis G, Zeng S, *et al*. Completely automated multi-resolution edge snapper. A new technique for an accurate carotid ultrasound IMT measurement: Clinical validation and benchmarking on a multi-institutional database. IEEE Trans. Image Proces. 2012; 21: 1211-22.

[24] Mechon-Lara RM, Bastida-Jumila MC, Morales-Sanchez J, *et al.* Automatic detection of the intima-media thickness in ultrasound images of the common carotid artery using neural networks. Med. Biol. Eng. Comput. 2014; 52(2): 169-81. PMid:24281725. http://dx.doi.org/10.1007/s11517-013-1128-4

[25] Petroudi S, Loizou CP, Pantziaris M, *et al.* Segmentation of the common carotid intima-media complex in ultrasound images using active contours. IEEE Trans. Biomed. Eng. 2012; 59(11): 3060-9. PMid:22922689. http://dx.doi.org/10.1109/TBME.2012.2214387

[26] Xu X, Zhou Y, Cheng X, *et al.* Ultrasound intima-media segmentation using Hough transform and dual snake model. Comp. Med. Imag. Graph. 2012; 36: 248-58. PMid:21741209. http://dx.doi.org/10.1016/j.compmedimag.2011.06.007

[27] Bastida-Jumilla MC, Mechon-Lara RM, Morales-Sanchez J, *et al.* Segmentation of the common carotid artery walls based on a frequency implementation of active contours. J. Digit. Imaging. 2013; 26(1): 129-39. PMid:22552539. http://dx.doi.org/10.1007/s10278-012-9481-7

[28] Cheng J, Li H, Fenster A, *et al.* Fully automatic plaque segmentation in 3D ultrasound images. Ultr. Med. Biol. 2013; 39(2): 2431-46. PMid:24063959. http://dx.doi.org/10.1016/j.ultrasmedbio.2013.07.007

[29] Ukwatta E, Yuan J, Buchanan D, *et al.* Three-dimensional segmentation of three-dimensional ultrasound carotid atherosclerosis using sparse field level sets. Medic. Phys. 2013; 40(5): 1-17. PMid:23635296. http://dx.doi.org/10.1118/1.4800797

[30] Ananey M, Mellotte G, Maher V. Comparison of semi-automated and manual measurements of carotid intima-media thickening. Bio. Med. Res. Intern. 2014: 1-4.

[31] Santos MF, Dos Santos RM, Castro PMAC, *et al.* A novel automatic algorithm for the segmentation of the lumen of the carotid artery in ultrasound B-mode images. Expert. Sys. & Applic. 2013; 40: 6570-79. http://dx.doi.org/10.1016/j.eswa.2013.06.003

[32] Loizou P, Pantziaris M, Pattichis MS, *et al*. Pattichis, Ultrasound image texture analysis of the intima and media layers of the common carotid artery and its correlation with age and gender. Comput. Med. Imag. Graph. 2009; 33(4): 317-24. PMid:19304453. http://dx.doi.org/10.1016/j.compmedimag.2009.02.005

[33] Loizou P, Petroudi S, Pattichis CS, *et al*. Nicolaides, An integrated system for the segmentation of atherosclerotic carotid plaque in ultrasound video. IEEE Trans. Ultras. Ferroel. Freq. Contr. 2014; 61(1): 86-101. PMid:24402898. http://dx.doi.org/10.1109/TUFFC.2014.6689778

[34] Loizou P, Pantziaris M, Pattichis CS, *et al.* M-mode state-based identification in ultrasound videos of the common carotid artery. Proc. 4th Int Symp Commun Contr & Sign Proces, ISCCSP, Limassol, Cyprus; 2010. p6.

[35] Lee J.S. Refined filtering of image noise using local statistics. Comp. Graph. & Image Process. 1981; (15): 380-9.

[36] North American symptomatic carotid endarterectomy trial collaborators: Beneficial effect of carotid endarterectomy in symptomatic patients with high-grade carotid stenosis. N. Engl. J. Med. 1991; 325: 445-53. PMid:1852179. http://dx.doi.org/10.1056/NEJM199108153250701

[37] Williams J, Shah M. A fast algorithm for active contours and curvature estimation. Int. J. Graph. Vision. Imag. Proc.: Image Underst. 1992; 55: 14-26. http://dx.doi.org/10.1016/1049-9660(92)90003-L

[38] Metz C. Basic principles of ROC analysis. Semin. Nucl. Medic. 1978; 8: 283-98. http://dx.doi.org/10.1016/S0001-2998(78)80014-2

[39] Shapiro SS, Wilk MB. An analysis of variance test for normality (complete samples). Biometrika. 1965; 52: 3-4. http://dx.doi.org/10.1093/biomet/52.3-4.591

[40] Cohen J. Statistical power analysis for the behavioral sciences (2nd ed.) Hillsdale, NJ: Lawrence Earlbaum Associates. 1998.

[41] Bots ML, Hoffman A, Diederick EG. Increased common carotid intima-media thickness. Adaptive response or a reflection of atherosclerosis? Findings from the Rotterdam Study. Stroke. 1997; 28: 2442-7. PMid:9412629. http://dx.doi.org/10.1161/01.STR.28.12.2442

[42] van der Meer M, Bots ML, Hofman A, *et al*. Predictive value of noninvasive measures of atherosclerosis for incident myocardial infarction: The Rotterdam Study. Circulation. 2004; 109(9): 1089-94. PMid:14993130. http://dx.doi.org/10.1161/01.CIR.0000120708.59903.1B

[43] Wendelhag Q, Liang T, Gustavsson JW. A new automated computerized analyzing system simplifies reading and reduces the variability in ultrasound measurement of intima media thickness. Stroke. 1997; 28: 2195-200. PMid:9368564. http://dx.doi.org/10.1161/01.STR.28.11.2195

[44] Puchner S, Reiter M, Baros C, *et al.* Assessment of intima-media thickness of carotid arteries: evaluation of an automated computer software. Neuroradiol. 2008; 50(10): 849-53. PMid:18548241. http://dx.doi.org/10.1007/s00234-008-0405-7

[45] Yanase T, Nasu S, Mukuta Y, *et al.* Evaluation of a new carotid intima-media thickness measurement by B-Mode ultrasonography using an innovative measurement software, intimascope. Amer. J. Hypertens. 2006; 19(12): 1206-12. PMid:17161764. http://dx.doi.org/10.1016/j.amjhyper.2006.05.010

[46] Ananey M, Mellote G, Maher V. Comparison of semi-automated and manual measurements of carotid intima-media thickening. Biomed. Researc. Int. 2014: 1-4.

[47] Dogan S, Plantinga Y, Dijk JM, *et al.* Manual B-Mode versus automated radio-frequency carotid intima-media thickness measurements. J. Americ. Soc. Echogard. 2009; 22(10): 1137-44. http://dx.doi.org/10.1016/j.echo.2009.07.008

[48] Willekes C, Hoeks APG, Bots ML, *et al.* Evaluation of off-line automated intima-media thickness detection of the common carotid artery based on M-line signal processing. Ultras. Med. Biol. 1999; (25): 57-64.

[49] van Bortel LM, Vanmolkot FH, van der Heijden-Spek JJ, *et al.* Does B-mode common carotid artery intima-media thickness differ from M-mode? Ultr. Med. Biol. 2001; 27: 1333-6. http://dx.doi.org/10.1016/S0301-5629(01)00448-3

[50] Foley RN, Parfrey PS, Sarnak MJ. Clinical epidemiology of cardiovascular disease in chronic renal disease. Am. J. Kidney Dis. 1998; 32: 112-9. http://dx.doi.org/10.1053/ajkd.1998.v32.pm9820470

[51] Brzosko S, Lebkowska U, Malyszko J, *et al.* Intima media thickness of common carotid arteries is associated with traditional risk factors and presence of ischemic heart disease in hemodialysis patients. Physiol. Res. 2005; 54: 497-504. PMid:15641938.

[52] Drueke T, Witko-Sarsat V, Massy Z, *et al*. Iron therapy, advanced oxidation protein products, and carotid artery intima-media thickness in end-stage renal disease, Circulation. 2002; 106: 2212-7. PMid:12390950. http://dx.doi.org/10.1161/01.CIR.0000035250.66458.67

[53] Glagov S, Vito R, Giddens DP, *et al.* Micro-architecture and composition of artery walls: relationship to location, diameter and the distribution of mechanical stress. J. Hypertens. 1992; 10(6): S101-S104. http://dx.doi.org/10.1097/00004872-199208001-00026

[54] Jensen-Urstad M, Johansson J. Carotid artery correlates with risk factors for cardiovascular disease in a population of 55-year-old subjects. Stroke. 1999; 30(8): 1572-6. PMid:10436103. http://dx.doi.org/10.1161/01.STR.30.8.1572

[55] Bartels S, Franco AR, Rundek T. Carotid intima-media thickness (cIMT) and plaque from risk assessment and clinical use to genetic disorders. Perspectives in Medicine. 2012; 1: 139-45. http://dx.doi.org/10.1016/j.permed.2012.01.006

[56] Haralick RM, Shanmugam K, Dinstein I. Texture features for image classification. IEEE Trans. Syst. Man. Cyb. SMC. 1973; 3(6): 610-21. http://dx.doi.org/10.1109/TSMC.1973.4309314

[57] Loizou CP, Murray V, Pattichis MS, *et al.* Multiscale amplitude modulation-frequency modulation (AM-FM) texture analysis of ultrasound images of the intima and media layers of the carotid artery. IEEE Trans. Inf. Tech. Biomed. 2011; 15(2): 178-88. PMid:20889436. http://dx.doi.org/10.1109/TITB.2010.2081995

[58] Loizou CP, Theofanous C, Pantziaris M, *et al.* Despeckle filtering software toolbox for ultrasound imaging of the common carotid artery. Comput. Meth. Progr. Biomed. 2014; 114: 109-124. PMid:24560276. http://dx.doi.org/10.1016/j.cmpb.2014.01.018

[59] Loizou CP, Theofanous C, Pantziaris M, *et al*. Despeckle filtering toolbox for medical ultrasound video. Int. J. Monit. Surveil. Technol. Research (IJMSTR): Special issue Biomed. Monit. Technol. 2013; 4(1): 61-79.